

An experimental and theoretical study of $[\text{RhCl}(\text{PF}_3)_2]_2$ fragmentation

P. Seuret,^a F. Cicoira,^b T. Ohta,^b P. Doppelt,^c P. Hoffmann,^b J. Weber^a and T. A. Wesolowski^{*a}

^a Department of Physical Chemistry, University of Geneva, 1211, Geneva 4, Switzerland.
E-mail: Tomasz.Wesolowski@chiphys.unige.ch; Fax: +41 22 7026 532; Tel: +41 22 7026 957

^b Institute of Imaging and Applied Optics, Ecole Polytechnique Fédérale de Lausanne, 1015, Lausanne-EPFL, Switzerland

^c École Supérieure de Physique et de Chimie Industrielles de la Ville de Paris, 10 rue Vauquelin, 75231, Paris Cedex 02, France

Received 10th July 2002, Accepted 12th November 2002

First published as an Advance Article on the web 3rd December 2002

Experimental and theoretical techniques have been applied to study the decomposition of the $[\text{RhCl}(\text{PF}_3)_2]_2$ molecule which is known as a precursor in electron beam induced deposition (EBID) of Rh. Mass spectrometry (MS) has been carried out to study the electron ionisation and fragmentation of isolated molecules. Auger electron spectroscopy has been used to characterize the EBID deposit. The MS data indicate the presence of free phosphorus and rhodium ions. This is in agreement with the analysis of the composition of the EBID deposit containing: 60% Rh, 12–25% P, 2–13% Cl, no F, 3–20% O and N. Theoretical calculations (density functional theory) has been used to characterize the precursor molecule and to derive the enthalpies of several simple decomposition reactions. The calculated geometries are in a good agreement with the available X-ray crystallographic data. The $[\text{RhCl}(\text{PF}_3)_2]_2$ appears not to be rigid: the PF_3 groups can rotate with a relatively low barrier ($0.6 \text{ kcal mol}^{-1}$) whereas the barrier for the butterfly-like motion of $(\text{RhCl})_2$ moiety is only $3.5 \text{ kcal mol}^{-1}$. According to the theoretical results, the lowest energy pathway of the decomposition corresponds to a consecutive loss of PF_3 ligands, resulting in a $(\text{RhCl})_2$ moiety (without phosphorus). The same conclusion is also valid for the ionised precursor. Experimental data combined with the theoretical results concerning the energetics of the considered various simple decomposition processes indicate that the electron induced dissociation of the precursor cannot be seen as a simple one-step decomposition process.

Introduction

The $[\text{RhCl}(\text{PF}_3)_2]_2$ molecule is known as a precursor molecule for rhodium deposition in various chemical vapour deposition techniques. Thermal decomposition of $[\text{RhCl}(\text{PF}_3)_2]_2$ leads to pure Rh films.¹ This molecule is used also to obtain micro- and nanostructures by scanning tunnelling microscope assisted chemical vapour deposition and by electron beam induced deposition (EBID).^{2,3} The latter technique applies a focused electron beam (3 keV–25 keV) in a vacuum system to decompose precursor molecules. The precursor molecule is delivered onto a substrate in the gas phase. An ideal precursor for EBID should decompose to pure metal and easily evacuated volatile products. The most important properties of $[\text{RhCl}(\text{PF}_3)_2]_2$ as precursor for EBID are: (a) the absence of carbon, (b) the presence of the stable leaving groups (PF_3) as ligands, and (c) its high volatility.⁴ In this work, we apply several experimental and theoretical techniques to study the properties of $[\text{RhCl}(\text{PF}_3)_2]_2$ relevant to its fragmentation. Gas phase low pressure mass spectrometry (MS) is used for characterization of the precursor electron induced dissociation, whereas Auger electron spectroscopy (AES) is used to characterize the deposit obtained with a focused electron beam irradiating a surface exposed to higher pressures of the precursor. Density functional theory (DFT) modelling of the intact precursor molecule, its ionised forms and its fragments obtained in various simple “thermal” decomposition processes is used to provide data not directly available in our experiments.

In principle, theoretical modelling at the quantum mechanical level should provide a complete picture of the decomposition process. Due to the fact that this process occurs in

the far-from-equilibrium conditions and the participation of the interactions with the deposit on the surface can not be *a priori* excluded, modelling the whole decomposition process starting from first principles only is not a currently attainable objective.

Nevertheless, we applied DFT calculations to get such information as: (a) flexibility of the precursor molecule, (b) stability of its various fragments resulting from simple decomposition processes and (c) the relative energy of some model decomposition reactions. To check the reliability of the applied theoretical method (DFT) the structure of the neutral isolated precursor molecule was compared with the available structural data derived from X-ray crystallography and previous theoretical (not DFT) studies.

Materials and methods

Experimental

The experimental setup for mass spectrometry measurements is based on a commercial mass spectrometer (Extranuclear Laboratories Inc., Pittsburgh, USA), including an electron beam ioniser, focusing optics, a quadrupole mass filter and a channeltron electron multiplier. The spectrometer head is mounted in a UHV chamber, pumped with a turbo molecular pumping station (Pfeiffer TPH 170) with a nominal pumping speed of 170 l s^{-1} for N_2 . The ultimate pressure in the chamber, measured by means of a Bayard-Alpert gauge (Balzers IMG 070) is about $1 \times 10^{-7} \text{ Pa}$ ($1 \times 10^{-9} \text{ Torr}$). The precursor gas is injected into the detection chamber from a container through an injection line. The latter is linked to the UHV

chamber by means of a variable leak valve. During measurements the injection line is kept at 35 °C to avoid condensation of precursor molecules in the introduction system while the precursor container is kept at room temperature (regulated at 20 ± 1 °C) to minimize thermal decomposition. The current signal of the positive ion detector is read by a pico-ammeter (Keithley 485 Autoranging picoammeter, USA). The data are acquired by a personal computer through a data acquisition card (16-bit data acquisition card PCI-M10-16XE-10, National Instrument, Austin, USA), and stored on-line with a LabVIEW program (National Instrument, Austin, USA). The measurements are averaged over 50 acquisitions. Mass spectra of $[\text{RhCl}(\text{PF}_3)_2]_2^+$ have been acquired at three different ionising electron energies: 10 eV, 30 eV and 70 eV, with a constant electron current of 4.4 mA. In all experiments only positive ions were detected. The highest fragmentation efficiency has been observed at 70 eV while no change in the relative peak intensities has been detected for the three electron energies applied. Increased precursor pressure from 1.0×10^{-4} Pa to 2.0×10^{-4} Pa did not show any effect on the peak ratios.

Theoretical calculations

Density functional theory as implemented into the ADF2000.02 package^{5,6} is applied to study structure, flexibility and energetics of various simple decomposition processes relevant to thermal decomposition and eventually EBID of $[\text{RhCl}(\text{PF}_3)_2]_2^+$. Triple zeta basis functions with polarization (type IV basis set in ADF) is used in all calculations. The generalized gradient approximation (GGA) applying the Becke88 exchange⁷ and Perdew86 correlation⁸ functionals is used in most of the calculations. For some properties, local density approximation (LDA) is used for comparison purposes. The geometry optimisation is performed using the quasi Newton algorithm in its Broyden–Fletcher–Goldfarb–Shanno version with the following convergence criteria: $10^{-5} E_h$ for the energy change and $5 \times 10^{-3} E_h \text{ \AA}^{-1}$ for the energy gradient. In all the calculations (geometry optimisation, transition states and single point calculations), no explicit symmetry was enforced. Energy barriers (for PF_3 rotation, butterfly motion of the $(\text{RhCl})_2$ moiety, and the F_2 elimination from isolated PF_3) are evaluated by multiple single point calculations (butterfly motion of the Rh_2Cl_2 moiety and PF_3 rotation) or with the linear transit method.⁹ For each analysed decomposition process, the enthalpy of reaction is calculated as the total energy difference of relevant species at their optimised geometries. Unrestricted calculations are applied for paramagnetic species.

Results and discussion: Experimental part

Mass spectrometry

The mass spectrum of $[\text{RhCl}(\text{PF}_3)_2]_2^+$, with the assigned fragments, is shown in Fig. 1. The spectrum has been obtained using an ionisation energy of 70 eV and a precursor pressure of 2.0×10^{-4} Pa.

The principal peaks have been found at the mass numbers of 50, 69, 88 and 103. These masses correspond respectively to the ions P^+ , PF_2^+ , PF_3^+ and Rh^+ . The ratios between the main peaks are roughly the same in the spectra measured at different energy, *i.e.*: $\text{PF}_2^+:\text{PF}_3^+ \approx 1:2$; $\text{PF}_2^+:\text{P}^+ \approx 1:15$ and $\text{PF}_2^+:\text{Rh}^+ \approx 1:50$. It results therefore, that the ratio between $\text{P}^+:\text{Rh}^+ \approx 1:3$.

The peaks of the ions $\text{P}^+(31)$, $\text{Cl}^+(35)$ and $\text{F}_2^+(38)$ are clearly detected below 100 u. The most intense peaks are measured, at 69 u (PF_2^+) and at 88 u (PF_3^+), as already found by other authors for the spectrum of free PF_3 .¹⁰ Furthermore, the single Rh^+ peak appears at mass 103 with a large yield. The precursor molecular single charged mother peak is clearly observed at 628 u together with its isotopic peaks, due to the

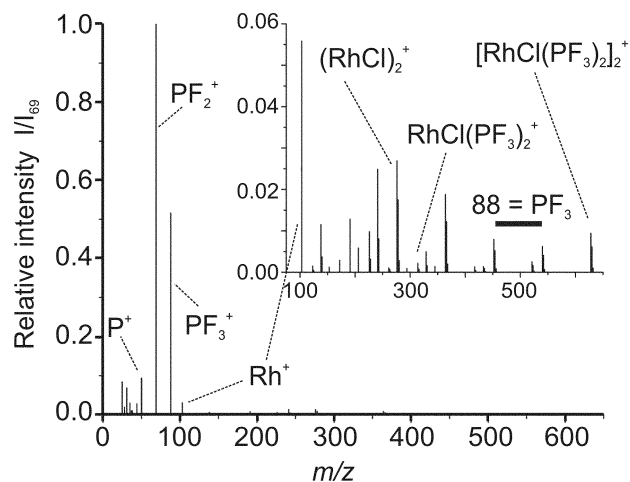


Fig. 1 Typical positive ion mass spectrum of $[\text{RhCl}(\text{PF}_3)_2]_2^+$, with the assigned fragments. The spectrum has been acquired at 70 eV electron energy. The precursor pressure during the acquisition was 1.5×10^{-6} Torr.

presence of two chlorine atoms, at 630 u and 632 u. The peaks generated by consecutive loss of PF_3 from the molecular peak are observed with increasing intensity in the order: $(\text{PF}_3)_3\text{Rh}_2\text{Cl}_2^+$, $(\text{PF}_3)_2\text{Rh}_2\text{Cl}_2^+$, $(\text{PF}_3)\text{Rh}_2\text{Cl}_2^+$ and Rh_2Cl_2^+ . Beside these peaks, the ones with the loss of one F atom, $(\text{PF}_2)(\text{PF}_3)_2\text{Rh}_2\text{Cl}_2^+$ and $(\text{PF}_2)(\text{PF}_3)\text{Rh}_2\text{Cl}_2^+$, have been observed. The peak at 345 u belongs to $(\text{PF}_2)\text{Rh}_2\text{Cl}_2^+$.

The MS results prove that the 70 eV electron irradiation decomposes efficiently the $[\text{RhCl}(\text{PF}_3)_2]_2^+$ molecule. Light fragments present at high yield, like PF_2^+ , PF_3^+ , P^+ , Cl^+ and Rh^+ reveal the strong fragmentation even into single ions under these experimental conditions. With much lower peak intensities the consecutive loss of PF_3 groups is also observed (see inset in Fig. 1). The latter indicates a weak Rh–P bond. The even lower intensity of the monomer peak indicates the strength of the Rh–Cl bond. Atomic F loss from PF_3 groups is monitored by the detection of 50% PF_2^+ compared to PF_3^+ and also from the peaks, $(\text{PF}_2)_3\text{Rh}_2\text{Cl}_2^+$, $(\text{PF}_2)_2\text{Rh}_2\text{Cl}_2^+$ and $(\text{PF}_2)\text{Rh}_2\text{Cl}_2^+$, and it seems to occur preferentially after the loss of one or two PF_3 ligands. The presence of a relatively intense Rh^+ peak is an indication of the suitability of the precursor for high content Rh EBID. It can be concluded that the obtained mass spectrum allows the prediction of a high Rh content EBID deposit with Cl contamination. The presence of P ions at low intensity is a first hint to phosphorus being included in the deposit. With the higher electron energy and orders of magnitude higher electron current densities in the EBID process, a further increase of single atom ions can be supposed.

Composition of the deposit

By focused electron beam induced decomposition of precursor molecules on the substrate functional deposits are obtained. The different limits of EBID are discussed in the literature.¹¹ In the case of $[\text{RhCl}(\text{PF}_3)_2]_2^+$ as precursor, fast growing deposits are obtained. *Ex-situ* Auger electron spectroscopy as well as transmission electron microscopy and high resolution electron energy loss spectroscopy were carried out to determine the chemical composition of the deposits and its structure.³ Metallic rhodium crystals with diameters of about 5 nm in an amorphous lighter material matrix are obtained. Electron energy loss spectroscopy reveals that the Rh rich regions are correlated with P rich regions, and the lighter rhodium free matrix contains O and N contamination. Fluorine has not been detected in the deposits. All AES results reveal about 60%

Rh, 12–25% P, 2–13% Cl, no F, 3–20 %O and N. This is a surprising result since the PF bond is known to be stronger than other bonds in $[\text{RhCl}(\text{PF}_3)_2]_2$. Therefore, more insight into the detail of the decomposition process is of crucial interest for the control of the physico-chemical properties of the deposit.

Results and discussion: Theoretical part

The presence of nitrogen and oxygen in the deposit reported in the previous section is probably related to post-deposit contamination. The presence of phosphorus and chlorine is, however, most likely due to a corresponding decomposition of the precursor.

The absence of fluorine in the deposit and a significant concentration of phosphorus is especially intriguing since the PF bond is rather strong. For instance, the experimental reaction enthalpy (ΔH_r) for the reaction $\text{PF}_3^+ \rightarrow \text{PF}_2^+ + \text{F}$ amounts to about 89 kcal mol⁻¹.¹⁰ To get additional insight into the decomposition process, we perform theoretical calculations. In the first part, we analyse the properties of the isolated $[\text{RhCl}(\text{PF}_3)_2]_2$ molecule and compare the obtained results with the experimental data. One of the objectives of this part is to test the adequacy of the chosen theoretical method (DFT-GGA). In the second part, we analyse the properties of the $[\text{RhCl}(\text{PF}_3)_2]_2$ molecule (neutral or ionised) which have not been measured directly, such as: its flexibility (barriers to the internal motions), structural stability of its fragments obtained in various decomposition processes and the enthalpies of various fragmentation processes. These reactions are related to the possible decomposition mechanism.

Structure of the precursor molecule

In this section, we compare the calculated structure of the free molecule $[\text{RhCl}(\text{PF}_3)_2]_2$ with the experimental solid state crystal structure obtained by Doppelt *et al.*¹² (see Fig. 2). The molecule contains two $(\text{PF}_3)_2\text{RhCl}$ units forming a butterfly-like moiety of the Rh and Cl atoms, forming a Rh–Cl–Rh angle of 113.5° (denoted as θ throughout this work). In this arrangement, the Rh–Rh distance is smaller compared to other dirhodium complexes ($[\text{RhCl}(\text{CO})_2]_2$: $\theta = 127^\circ$, $d_{\text{Rh–Rh}} = 3.12$ Å,¹³ $[\text{RhCl}(\text{PPh}_3)_2]_2$: $\theta = 180^\circ$, $d_{\text{Rh–Rh}} = 3.66$ Å¹⁴ and $[\text{cis-RhCl}(\text{CO})_2(\text{PMe}_2\text{Ph}_2)_2]_2$: $\theta = 125^\circ$, $d_{\text{Rh–Rh}} = 3.17$ Å¹⁵). The molecule has the C_{2v} symmetry in the crystal.

At the first stage, the geometry of isolated $[\text{RhCl}(\text{PF}_3)_2]_2$ was optimised at the LDA level. This structure was subsequently optimised at the GGA level. Table 1 shows that the change of the approximation for the exchange-correlation functional (from LDA to GGA) does not affect significantly the geometry

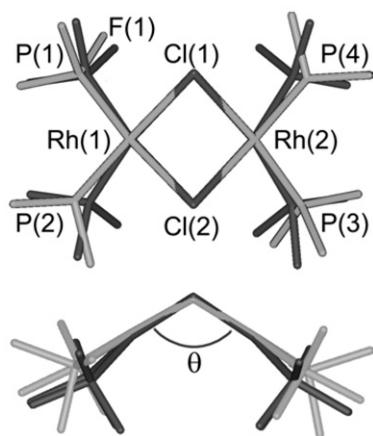


Fig. 2 X-ray crystallographic structure¹² (dark) and DFT-GGA optimised structure (light) of $[\text{RhCl}(\text{PF}_3)_2]_2$.

Table 1 The geometry of the $[\text{RhCl}(\text{PF}_3)_2]_2$ molecule derived from X-ray diffraction¹² and our calculations. The MP2 results¹⁷ for the $[\text{RhCl}(\text{PH}_3)_2]_2$ molecule are given for comparison. Bond distances are given in Angström and angles in degrees

Bond/angle	X-ray	MP2 ^a	LDA	GGA
Rh1–Cl1	2.395	2.446	2.373	2.429
Rh1–P1	2.124	2.192	2.136	2.181
P1–F1	1.525		1.586	1.606
Rh1–Rh2	2.971	3.059	3.024	3.142
Cl1–Cl2	3.195	3.294	3.183	3.219
Proximal F–F ^b	2.706		3.127	3.188
Distal F–F ^b	3.519		4.719	4.884
Cl1–Rh1–Cl2	83.8	84.6	84.5	83.0
Rh1–Cl1–Rh2	76.9	77.4	79.4	80.6
Cl1–Rh1–P1	89.9	92.0	89.7	93.6
Rh1–P1–F1	116.6		118.5	118.6
P1–Rh1–P2	94.0	91.3	92.0	93.4
P1–Rh1–Rh2–P4	–1.7		–2.2	0.76
Rh1–Cl1–Cl2–Rh2	113.6	115.5	119.2	119.6

^a Results for the $[\text{RhCl}(\text{PH}_3)_2]_2$ molecule; ^b The distance given in the table corresponds to the closest fluorine atoms belonging to different PF_3 groups.

and is in agreement with known tendencies reported for other organometallic complexes.¹⁶

We note here that a similar compound ($[\text{RhCl}(\text{PH}_3)_2]_2$) was included in a theoretical study at the MP2 *ab initio* level by Aullón *et al.*¹⁷ of various binuclear square planar complexes of d⁸ transition metal ions. The study by Aullón *et al.* led to a very similar geometry to that derived from X-ray measurements for $[\text{RhCl}(\text{PF}_3)_2]_2$ (see Table 1). In view of the discussion of the MP2 results,¹⁷ the bending distortion in DFT calculations (6°) is probably due to the underestimation of the rhodium d_{z²}/p_z overlap stabilization effect.

At the optimised geometry, the C_{2v} symmetry observed in X-ray is lowered by rotation of two PF_3 groups into C_2 symmetry (both at LDA and GGA levels). We attribute this effect to the crystal packing forces, which can result in a rotation of the PF_3 groups (see below).

Opposite to the geometry, the GGA relative energies are usually significantly more accurate than those derived from LDA.¹⁶ Therefore, GGA is used in all further analyses.

Flexibility of the precursor molecule

The barrier to the rotation of the PF_3 groups about the Rh–P bonds can be expected to be rather low because those groups are relatively distant and the Rh–P bond has a single σ character. The calculated potential energy curve for the rigid rotation of a PF_3 group where all the other degrees of freedom were kept constant indicates the upper bond for the transition state to be 1.8 kcal mol⁻¹. This barrier is significantly lowered (to about 0.6 kcal mol⁻¹) if the other parts of the molecule are allowed to vary (flexible rotation).

Changes of the Rh–Cl–Cl–Rh θ dihedral angle result in a butterfly-like movement of the whole molecule. Using the same method of rigid exploration of conformational space, the butterfly-like potential energy curve is calculated. The maximum on this curve corresponds to a planar arrangement ($\theta = 180^\circ$) with an energy of 3.5 kcal mol⁻¹ with a maximum at $\theta = 180^\circ$ whereas the energy minimum corresponds to 119.6°.

Decomposition of the neutral precursor molecule

In this part, various decomposition channels of the neutral molecule are analysed. In view of the key question revealed in the experimental part, namely the absence of fluorine in the deposit and a significant concentration of the phosphorus,

we study the enthalpies of fragmentation in various single-step decomposition processes. The reference for the discussion of various decomposition channels is the enthalpy of reaction in direct F₂ elimination reaction from the whole molecule (or from the isolated PF₃). Energy differences correspond to the separately optimised species.

The first considered decomposition scenario consists of successive eliminations of PF₃ groups followed by the elimination of F₂ molecules from PF₃.

The second scenario consists of the direct elimination of F₂ molecules from the whole [RhCl(PF₃)₂]₂ molecule.

Finally, two other fragmentation reactions are studied. The first is the symmetrical separation in two RhCl(PF₃)₂ "monomers" and the second is an asymmetrical breaking leading to the RhCl₂(PF₃)₂ and Rh(PF₃)₂ products.

Table 2 lists the considered reactions and the corresponding reaction enthalpies. This table introduces also the reaction labels used throughout the text.

Fragmentation of [RhCl(PF₃)₂]₂ via PF₃ removal

There are four PF₃ groups in the precursor molecule and the enthalpies of the reaction of each elementary PF₃ removal reaction might depend on the order of the elimination process. Fig. 3 shows the enthalpies of reactions obtained in such processes. The energy of the single PF₃ group removal from the intact precursor or from Rh₂Cl₂(PF₃)₃ does not strongly depend on the position of the PF₃ groups bound to the (RhCl)₂ moiety ($32 < \Delta H_r < 46$ kcal mol⁻¹). This can be seen as evidence for a rather low delocalisation of the electrons on the whole molecule and it explains the lack of cooperativity in the PF₃ elimination reactions. Such interpretation is further

supported by an apparent structural stability of the (RhCl)₂ moiety. As shown in Table 3, the elimination of any PF₃ group results in only a modest geometry deformation.

Note, however, that the elimination of the first two PF₃ groups cost about 10 kcal mol⁻¹ more than the subsequent eliminations. This results mostly from the slight differences in the structural relaxation of the decomposition fragments. In the case of the elimination of the first and the second PF₃, the energy change accompanying the geometric relaxation amounts less than 2 kcal mol⁻¹. For the subsequent PF₃ eliminations, this effect amounts to about 7 kcal mol⁻¹.

The calculated energy needed to break a P–Rh bond in [RhCl(PF₃)₂]₂ (39–48 kcal mol⁻¹) is about two times lower than the energy needed to break the P–Rh bond energy in the diatomic derived from the experimental measurements (84 ± 4 kcal mol⁻¹¹⁸). This difference in the bond strength can be explained by the presence of fluorine and chlorine atoms. The high electronegativity of those halogens induces a significant withdrawal of electrons and thus a destabilization of the Rh–P bond.

The potential energy curve corresponding to elongation of the Rh–P distance (Fig. 4) is monotonic *i.e.* no barrier is detected for the recombination reaction.

F₂ elimination from the isolated PF₃ (reactions 1 and 2)

In the decomposition scenario analysed in this part, the PF₃ groups are intermediate products. The absence of fluorine and the presence of phosphorus in the deposit requires, therefore, a further elimination of fluorine from PF₃. We consider two possible pathways for the PF₃ decomposition: reactions 1 and 2 in Table 2. The linear transit procedure applied to

Table 2 Degradation pathways of the neutral molecules considered in this study and the calculated ΔH_r values

	Reaction path	$\Delta H_r/\text{kcal mol}^{-1}$
1 ^a	PF ₃ → F ₂ + PF ^{••}	190
2 ^a	PF ₃ → F ₂ + PF	213
3 ^b		215
4 ^b		192
5 ^b		385
6 ^c		85
7 ^c		48
8 ^d		123
9 ^d		558

^a Elimination of a F₂ molecule from an isolated PF₃ group. ^b Direct elimination of fluorine molecules. ^c Symmetric reaction pathway. ^d Asymmetric reaction pathway and the calculated associated energy. The energy of the ionic pathway is significantly destabilized by the Rh(PF₃)₂²⁺ product which is about 500 kcal mol⁻¹ less stable than the biradical one while the RhCl₂(PF₃) part is more stable in its ionic form (78 kcal mol⁻¹).

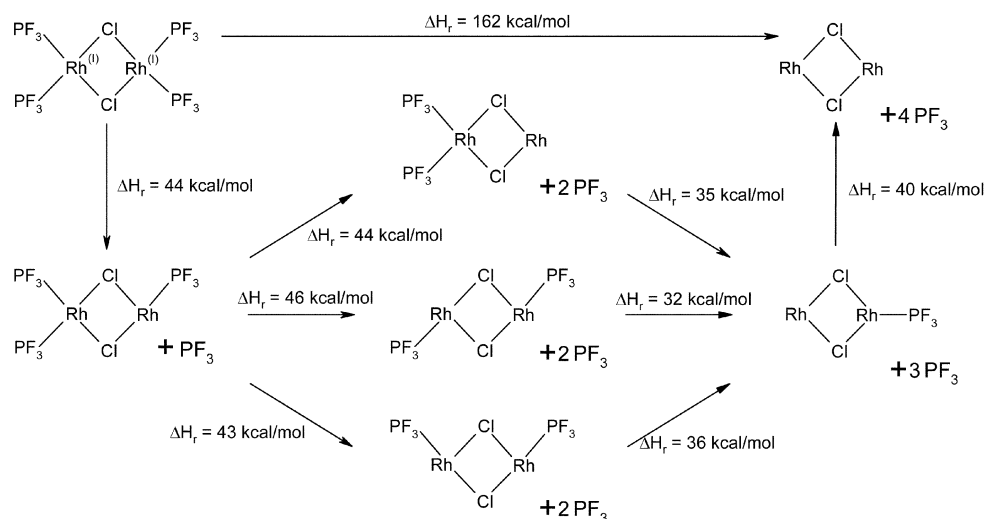


Fig. 3 Different successive reactions of PF₃ elimination and the associated energies.

determine the potential energy curve in this reaction shown in Fig. 5 is monotonic indicating no barrier for the recombination reaction.

The other decomposition channel considered here, reaction 1, involves the biradical product (PF^{••}). The enthalpy of this reaction is slightly lower (190 kcal mol⁻¹).

Compared to the energy needed to break the P–Rh bonds in the previous stages of this scenario, the energy needed to break the PF₃ molecule following reactions 1 and 2 is significantly higher.

Fragmentation of [RhCl(PF₃)₂]₂ via direct F₂ elimination (reactions 3–5)

We consider two possible pathways for the elimination of the F₂ molecule from the precursor: one in which two fluorine atoms from the same PF₃ group are eliminated (reaction 3) and the other one, in which two eliminated fluorine atoms belong to two different neighbouring PF₃ groups (reaction 4).

In both cases, the subsequent elimination of the second F₂ molecule leads to the same double biradical molecule (reaction 5).

ΔH_r of the first F₂ elimination following reaction 4 amounts to 192 kcal mol⁻¹ whereas that following reaction 3 amounts to 215 kcal mol⁻¹.

As the elimination of two F₂ molecules is concerned (reaction 5), it is worthwhile noting that its energy cost is about twice that of reaction 4. Moreover, it is important to underline that the enthalpies of reactions 1 and 4 are almost the same (190 and 192 kcal mol⁻¹). The similar observation can be made for reactions 2 and 3. This indicates that the interaction between the PF₃ group and the (RhCl)₂ moiety negligibly affects the energy of the F₂ elimination reaction. The isolated PF₃ molecule can be, therefore, considered as a simplified

Table 3 The geometry parameters for the optimised intact precursor molecule ([RhCl(PF₃)₂]₂) and the (RhCl)₂ decomposition fragment. Bond distances are given in Ångströms and angles in degrees

Bond/angle	[RhCl(PF ₃) ₂] ₂	Rh ₂ Cl ₂
Rh–Cl	2.428	2.326
Rh–Rh	3.142	2.558
Rh–Cl–Rh	80.6	66.7
Cl–Rh–Cl	83.0	105.2
Rh–Cl–Cl–Rh (θ)	119.6	129.7

but representative model for studies of F₂ elimination from the whole precursor molecule.

Fragmentation of [RhCl(PF₃)₂]₂ via breaking Rh–Cl bonds (reactions 6–9)

The Rh–Cl bonds can be broken in a homolytic or heterolytic way. The former one leads to the formation of two radical products (reaction 6) while the latter leads to a positive charge on the rhodium atoms and a negative charge on the chlorines (reaction 7). Table 2 shows that ionic fragmentation products are more stable. It is worthwhile to notice that the difference in electronegativity between the rhodium and chlorine atoms ($\Delta\text{electronegativity} = 0.88$, 19% ionic) is not too high and cannot, alone, explain this difference in stability.

The optimised geometry of the RhCl(PF₃)₂ fragment is very similar to that of the intact precursor. The rhodium is almost square planar indicating that its electronic configuration is conserved. Also, Mulliken population analysis of the charges shows only a slight difference of the positive charge on the rhodium in products of reactions 6 and 7 (+0.47 vs. +0.59 e). The unpaired electrons resulting from the homolytic fragmentation are essentially localized on the rhodium atom (spin density of 1.29 e) although a non-negligible spin density is localized on the chlorine and phosphorus (–0.38 and 0.13 e, respectively). These two configurations are the consequence of the tendency of unpaired electrons to occupy the orbitals localized on rhodium in order to stabilize such an electronic configuration where the number of electrons in the valence shell is as close as possible to 16.

The low fragmentation energy of reaction 7 seems to contradict the low intensity of its product MS peak (see Fig. 1). The

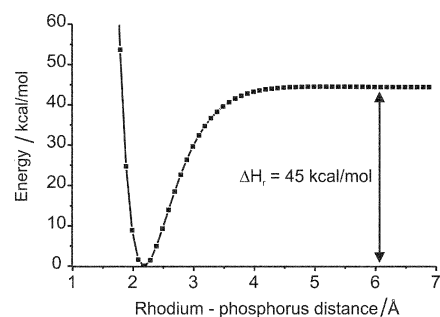


Fig. 4 The potential energy curve corresponding to the PF₃ elimination (of the group labelled as P(1) in Fig. 2).

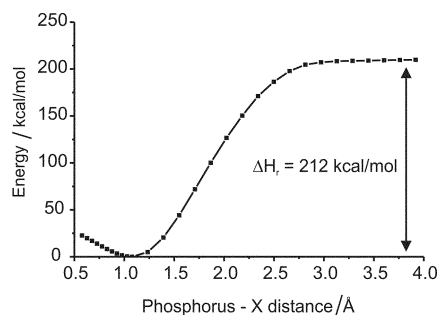


Fig. 5 The potential energy curve - corresponding to the elimination of F_2 from an isolated PF_3 molecule. X denotes the centre of mass of the F_2 molecule.

intensity is similar to the first PF_3 elimination but is far smaller than the $(PF_3)Rh_2Cl_2$ for example. The low amount of detected $(PF_3)_2RhCl$ ion is probably due to the stability of this species. This fragmentation product is probably easily degraded into smaller fragments with a short life-time in the MS experiment. Calculations also show that the energy cost for a single PF_3 elimination from the $RhCl(PF_3)_2$ fragment ($\Delta H_r = 43 \text{ kcal mol}^{-1}$) is similar to that for the PF_3 elimination from the intact precursor discussed in the previous section.

We proceed now to other fragmentation pathways also involving breaking Rh-Cl bonds (reaction 8—homolytic fragmentation or reaction 9—ionic fragmentation). Contrary to the case of reactions 6 and 7, the biradical fragmentation products are more stable than the ionic products. This results from the destabilising effect of the double positive charge of the ionic fragments (see Table 2). Moreover, the stabilizing effect of the 16 valence electrons discussed previously can not take place here.

Based on our results concerning the Rh-Cl bond breaking, we conclude that, compared to the 45 kcal mol^{-1} necessary for the elimination of a PF_3 group, the only competitive fragmentation reaction is the symmetric fragmentation (reaction 7) with $\Delta H_r = 48 \text{ kcal mol}^{-1}$.

Fragmentation of the ionised molecules

As the electron beam induces strong ionisation conditions by electron elimination, precursor molecules can be expected to occur in their ionised state. In this section, we parallel the results presented previously with the ones concerning the decomposition of the ionised precursor. We start with the analysis of the ionisation energy which is followed by the study of various fragmentation pathways. We limit our analysis to such fragmentation channels which were found in the previous section as those involving the lowest energy expenditure *i.e.* F_2 elimination from PF_3 and the PF_3 elimination from the precursor molecule. Similar to the calculations made for the neutral molecules, the energy of the selected reactions is calculated using optimised geometries.

Ionisation of the precursor molecule and its fragments

The calculated ionisation energy of the $[RhCl(PF_3)_2]_2$ molecule, determined as the energy difference between the neutral and ionised forms, equals $193 \text{ kcal mol}^{-1}$. This value is in reasonable agreement with the measurements by Nixon *et al.*¹⁹ ($207 \text{ kcal mol}^{-1}$). The calculated ionisation energy of the PF_3 molecule, which was considered in the previous sections as one of the possible intermediary fragmentation products equals $278 \text{ kcal mol}^{-1}$. This value is in a very good agreement with the experimental PF_3 ionisation energy derived from mass spectrometry measurements: $262\text{--}276 \text{ kcal mol}^{-1}$ by Hardland *et al.*²⁰ and $265\text{--}276 \text{ kcal mol}^{-1}$ by Torgerson and Westmore.¹⁰

Table 4 Influence of PF_3 ionisation on the enthalpy of F_2 elimination and the molecule structure. The parameter d is the distance between the P and the plane formed by fluorine atoms

Reaction	$\Delta H_r / \text{kcal mol}^{-1}$	Ionisation energy / kcal mol^{-1a}	Planarity parameter $d / \text{\AA}$
2 $PF_3 \rightarrow PF + F_2$	213	—	0.81
10 $PF_3^+ \rightarrow PF^+ + F_2$	184	279	0.55
11 $PF_3^{+2} \rightarrow PF^{+2} + F_2$	132	433	0.00
12 $PF_3^{+3} \rightarrow PF^{+3} + F_2$	163	740	0.01

^a Calculated for each successive PF_3 ionisation.

The energy of the successive ionisations of PF_3 grows quickly and not linearly (Table 4). The energy necessary for the F_2 elimination initially decreases upon the ionisation of the PF_3 molecule and then increases again (the minimum corresponds to PF_3^{+2} ion).

F_2 elimination from the isolated PF_3^+

Table 4 shows that the more electrons that are removed, the more planar is the geometry of the PF_3^{+x} molecule. The distance between phosphorus and the centre of mass of the three fluorine atoms decreases from 0.81 \AA in the neutral state to 0.00 \AA following double ionisation. This structure modification is associated with a strong destabilization of the PF_3 molecule which follows the depletion of the lone pair on the phosphorus atom. On the other hand, the fragmentation energy decreases from 213 to $132 \text{ kcal mol}^{-1}$ for a positive charge of $+2$. This results from the greater destabilization of the reactant compared to the destabilisation of the products upon ionisation. This difference of stability is probably due to the strong electronegativity of fluorine atoms which withdraw electrons from the phosphorus atom. This results in a greater energy cost of the ionisation of PF_3 compared to PF .

The calculated first ionisation energy ($279 \text{ kcal mol}^{-1}$) and PF bond lengths of PF_3^+ (1.56 \AA) and PF_3 (1.63 \AA) are in a good agreement with the recent Gaussian-3 and Gaussian-3X results of Lau and Li²¹ who reported the first ionisation energy equal to $264 \text{ kcal mol}^{-1}$ and the P-F distance equal to 1.58 \AA and 1.51 \AA for neutral and PF_3^+ respectively.

Fragmentation of $[RhCl(PF_3)_2]_2^+$ via PF_3 removal

We consider here the series of reactions at PF_3 in elimination from the ionised precursor ($[RhCl(PF_3)_2]_2^+$). The reactions are similar to the ones shown in Fig. 3. The heats of corresponding reactions are not significantly affected by the ionisation process. The maximum difference between the heats of reactions amounts to 8 kcal mol^{-1} for the $Rh_2Cl_2(PF_3)_3^+ \rightarrow Rh_2Cl_2(PF_3)_2^+ + PF_3$ and $Rh_2Cl_2(PF_3)_3 \rightarrow Rh_2Cl_2(PF_3)_2 + PF_3$ reactions.

Conclusion

The experimental studies reported in this work reveal that the $[RhCl(PF_3)_2]_2$ molecule in the EBID conditions forms a deposit which is not pure metal and which contains a significant concentration of phosphorus and not a detectable concentration of fluorine. The absence of fluorine and the presence of phosphorus in the deposit prompted our more detailed theoretical analysis of various simple decomposition processes and of the properties of the precursor molecule.

As far as the isolated precursor molecule is concerned, it was shown that the $[RhCl(PF_3)_2]_2$ molecule is quite flexible—the PF_3 groups can rotate almost freely and the global

“butterfly-like” motion of the (RhCl)₂ moiety involves also a rather low barrier.

Energetics of various simple fragmentation processes involving (a) elimination of the whole PF₃ groups, (b) elimination of F₂ molecules, and (c) breaking the Rh–Cl bonds in both the neutral and the ionised precursor molecule were studied theoretically. These studies showed that the direct elimination of fluorine which could lead to the absence of this atom in the deposit remains the most energetically expensive decomposition channel. The lowest energy decomposition pathway corresponds to a consecutive loss of PF₃ ligands, resulting in a (RhCl)₂ fragment which does not contain phosphorus but its geometry is almost the same as in the intact precursor. The same scenario appears also for the ionised precursor. This leads us to the conclusion that the absence of fluorine in the deposit results either from multiple ionisation by electron impact, or secondary reactions not included in our studies such as (a) the recombination of the highly reactive species (radicals) obtained in the primary decomposition process, (b) the interactions with the heterogeneous solid deposit. For instance, elimination of the fluorine atoms and phosphorus rich deposit could happen *via* the combination of PF₃ molecules to form PF₆ and free P. In this scenario, the unstable PF₆ could quickly convert to stable PF₅ and volatile F₂ products.

It is important, however, to underline that our theoretical analysis is limited to a quasi-stationary picture of the decomposition process *via* metastable intermediates. The energy available in both the mass spectroscopy (70 eV) as well as EBID experiments (beam of electrons scattered from the surface and generated by the primary beam of 3–25 keV) is very high compared to the energy differences in the bond breaking reactions considered in this study.

Finally, we turn back to the thermal decomposition of [RhCl(PF₃)₂]₂ which was reported in the literature to lead to pure Rh films.¹ In agreement with experiment, our DFT calculations show that the lowest energy fragmentation pathway consists of successive breaking of Rh–P and Rh–Cl bonds thus leading to the pure metal.

Acknowledgements

This study was supported by the Swiss National Science Foundation projects 21-64064.00 and 20-63496.00. The CPU grant

from the Swiss Center for Scientific Computing in Manno is greatly acknowledged.

References

- 1 P. Doppelt, V. Weigel and P. Guinot, *Mater. Sci. Eng.*, 1993, **B17**, 143–146.
- 2 F. Marchi, D. Tonneau, H. Dallaporta, R. Pierrisnard, V. Bouchiat, V. I. Safarov, P. Doppelt and R. Even, *Microelectron. Eng.*, 2000, **50**, 59–65.
- 3 F. Cicoira, PhD thesis, 2002, EPFL Lausanne, Switzerland.
- 4 T. Ohta, F. Cicoira, P. Doppelt, L. Beitone and P. Hoffmann, *Chem. Vap. Deposition*, 2001, **7**, 33–37.
- 5 E. J. Baerends, D. E. Ellis and P. Ros, *Chem. Phys.*, 1973, **2**, 41–51.
- 6 C. Fonseca Guerra, J. Snijders, T. Velde and E. Baerends, *Theor. Chem. Acc.*, 1998, **99**, 391–403.
- 7 A. D. Becke, *Phys. Rev. A*, 1988, **38**, 3098–3100.
- 8 J. P. Perdew, *Phys. Rev. B*, 1986, **33**, 8822–8824.
- 9 T. Velde, F. Bickelhaupt, E. Baerends, C. Fonseca Guerra, S. van Gisbergen, J. Snijders and T. Ziegler, *J. Comput. Chem.*, 2001, **22**, 931–967.
- 10 D. F. Torgerson and J. B. Westmore, *Can. J. Chem.*, 1975, **53**, 933–938.
- 11 P. Hoffmann, I. Utke and F. Cicoira, *Proceedings of the 10th International Conference on Nanoscience and Technologies*, St. Petersburg, 2002.
- 12 P. Doppelt, L. Ricard and V. Weigel, *Inorg. Chem.*, 1993, **32**, 1039–1040.
- 13 L. F. Dahl, C. Martell and D. L. Wampler, *J. Am. Chem. Soc.*, 1961, **83**, 1761–1762.
- 14 M. D. Curtis, W. M. Butler and J. Greene, *Inorg. Chem.*, 1978, **17**, 2928–2931.
- 15 J. J. Bonnet, Y. Jeannin, P. Kalck, A. Maisonnat and R. Poilblanc, *Inorg. Chem.*, 1975, **14**, 743–747.
- 16 T. Ziegler, in *Density-functional Methods in Chemistry and Material Science*, ed. M. Springborg, John Wiley & Sons, New York, 1997, ch. 4, p. 69–103.
- 17 G. Aullón, G. Ujaque, A. Lledos, S. Alvarez and P. Alemany, *Inorg. Chem.*, 1998, **37**, 804–813.
- 18 S. Smoes, R. Huguet and J. Drowart, *Z. Naturforsch. A*, 1971, **26**, 1934–1935.
- 19 J. F. Nixon, R. J. Suffolk, M. J. Taylor, J. G. Norman, Jr., D. E. Hoskins and D. J. Gmur, *Inorg. Chem.*, 1980, **19**, 810–813.
- 20 P. W. Hardland, D. W. H. Rankin and J. C. J. Thynne, *Int. J. Mass Spectrom. Ion Phys.*, 1974, **13**, 395–410.
- 21 J. K.-C. Lau and W. K. Li, *THEOCHEM*, 2002, **578**, 221–228.